ELSEVIER

Marine Geology 242 (2007) 271 – 289

MARINE GEOLOGY
INTERNATIONAL JOURNAL OF MARINE GEOLOGY, GEOCHEMISTRY AND GEOPHYSICS

www.elsevier.com/locate/margeo

Pb and other ore metals in modern seafloor tectonic environments: Evidence from melt inclusions

Yannick Beaudoin [a,*], Steven D. Scott [a], Michael P. Gorton [a], Zoltan Zajacz [b], Werner Halter [b]

[a] *Scotiabank Marine Geology Research Laboratory, Department of Geology, University of Toronto, 22 Russell St, Toronto, Ontario, Canada, M5S 3B1*

[b] *Isotope Geochemistry and Mineral Resources, Department of Earth Sciences, Swiss Federal Institute of Technology, ETH Zentrum NO, CH-8092 Zürich, Switzerland*

Received 20 April 2006; received in revised form 1 April 2007; accepted 4 April 2007

Abstract

Many modern seafloor tectonic environments are host to hydrothermal systems and associated polymetallic sulfide deposits. Metal transport and precipitation are controlled by magmatic processes such as pre-eruptive degassing and the hydrothermal cycle. The original availability of Pb and other ore metals in a given setting is dependent on concentrations in the original magmatic source or additional enrichment processes. We have examined the Pb budget of melt inclusions from nine modern seafloor settings representing back-arcs, mid-ocean ridges and seamounts. Melt inclusions provide information on the characteristics of parental magmas, including insights into metal budgets. Trace element data in melt inclusions hosted in plagioclase, olivine and pyroxene were obtained by laser-ablation inductively-coupled mass-spectrometry.

Results from back-arcs emphasize the impact of slab-subduction and dehydration processes on the chemical characteristics of generated magmas. Volatile- and fluid-mobile element-rich melt inclusions at Manus basin and Okinawa trough reflect a robust contribution of elements from the subducting slab as evidenced by relatively low Ce/Pb ratios. At Bransfield strait, on the other hand, melt inclusions are volatile poor, and fluid-mobile element ratios are similar to mid-ocean ridge values indicating little or no contribution from the slab. High Cu concentrations at Manus basin and Okinawa trough can be explained by fluxing of ferric iron from the subducting slab benefiting the production of sulfate over sulfide.

Metal budgets for seamounts located on and nearby the axis of mid-ocean ridge segments appear to be independent of any input of mantle plume material. Results from the southern Explorer ridge (strong lower mantle influence, transitional- and enriched-MORBs), Pito and Axial seamounts (moderate lower mantle influence, transitional-MORBs) and a Foundation near-ridge seamount (little to no mantle influence, normal-MORB) show that, despite similar tectonic environments and varying contributions of mantle plume material, Cu, Zn and Pb values do not vary significantly between the enriched and non-enriched magma components of a given setting.
© 2007 Elsevier B.V. All rights reserved.

Keywords: Pb; melt inclusions; LA-ICP-MS; back-arcs; mid-ocean ridges; seamounts

* Corresponding author. Now at UNEP-GRID Arendal, Teaterplassen 3, 4836 Arendal, Norway. Fax: +47 37035050.
E-mail address: yannick.beaudoin@grida.no (Y. Beaudoin).

0025-3227/$ - see front matter © 2007 Elsevier B.V. All rights reserved.
doi:10.1016/j.margeo.2007.04.004

1. Introduction

Melt inclusions have emerged as a significant tool for the study of magma genesis in modern seafloor environments. They are commonly used to provide insight into the characteristics of magmas prior to the influences of processes such as mixing and degassing. Melt inclusion chemistry can be used to reconstruct the evolution of host magmas through the interpretation of various element patterns (Sobolev and Shimizu, 1994; Sours-Page et al., 1999). These patterns define the compositions of erupted lavas including the concentration of metals that may be a potential source of hydrothermal sulfide deposits.

Many recent studies have examined melt inclusions in specific tectonic settings with an emphasis on the relationships between spreading rate and chemical variability, mantle temperature and crustal thickness (e.g., Sobolev et al., 1992; Sinton et al., 1993; Sobolev and Shimizu, 1993; Sobolev et al., 1994; Sobolev and Shimizu, 1994; Nielsen et al., 1995; Sours-Page et al., 1999; Shimizu et al., 2000; Michael et al., 2002). This study compares melt inclusion compositions from 9 different modern seafloor sites representing 4 different tectonic settings in an examination of magma ore metal budgets and their viability to be a metal source for hydrothermal sulfide deposits.

Attention is given to Cu, Zn and in particular Pb and the potential of a parent magma to be a source of the metals. Melt inclusion studies in the Manus basin back-arc have emphasized a magmatic contribution of metals in the formation of volcanogenic massive sulfide-type hydrothermal deposits (Yang and Scott, 1996; Kamenetsky et al., 2001; Yang and Scott, 2002, 2005, 2006). The ore metals Cu, Zn, Au, Ag and Ni have been observed and to some extent quantified in pre-eruption trapped inclusions. Pb has been less studied due to its low concentration in melt inclusions requiring detection limits previously unavailable by conventional microbeam analytical techniques except for SIMS. Pb behavior in modern seafloor systems has therefore remained poorly understood. This study focuses on determining the availability of Pb and other ore metals in parental magmas for settings that host sulfide deposits but does not attempt to consider the transfer of metals from the magmatic to the hydrothermal system. It is an attempt to put into context on-going work involving the potential for the direct magmatic contribution of Pb and other metals to metallic sulfide ores in volcanic terrain.

2. General geology of study sites

Site locations are numbered as in Fig. 1. Specific characteristics for each site are briefly presented below. Except where indicated, average Pb, Zn and Cu analyses of the hydrothermal deposits are for random samples as tabulated by Scott (1997).

2.1. Mid-Atlantic Ridge (MAR): TAG and Snake Pit hydrothermal areas

Basalt samples from two sites along the MAR were included in this study as representatives of a typical mid-ocean ridge spreading system having a slow rate of spreading. Both sample locations are characterized by N-MORB volcanism (Petersen et al., 2000).

The Trans-Atlantic Geotraverse (TAG) ridge segment extends from 25°55′N to 26°17′ N along the MAR slowly spreading asymmetrically at 1.3 cm to the east and 1.1 cm to the west (Purdy et al., 1990; Sempéré et al., 1990; McGregor et al., 1977). The hydrothermally active TAG mound (approximately 200 m in diameter) located at 26°08′ N latitude is at a juncture between the MAR valley floor and the eastern wall (Rona et al., 1986; Thompson et al., 1988).

Deposits at TAG are dominated by Cu- and Zn-sulfide assemblages. Fifty-nine samples averaged 0.04 wt.% Pb, 25.2 wt.% Zn and 6.3 wt.% Cu. Numerous studies of active and fossil sulfide deposits at, and in the vicinity of, the TAG field have described in detail the compositions and morphology of both low and high temperature systems (e.g., Rona et al., 1986; Thompson et al., 1988; Lisitsyn et al., 1989; Rona et al., 1993a,b; Bogdanov et al., 1995; Rona et al., 1996; Petersen et al., 2000).

The Snake Pit hydrothermal field is located at 23°22′ N latitude on the Mid-Atlantic Ridge. In contrast to the TAG field, Snake Pit occurs in the center of the axial valley on a north–south trending neovolcanic ridge (Fouquet et al., 1993). The main sulfide mound covers a 150 m by 300 m area. The surface of the mound is dominated by Zn-rich assemblages and the core by Cu-rich assemblages (Fouquet et al., 1993). Thirty-one samples from the mound averaged 0.07 wt.% Pb, 7.0 wt.% Zn and 12.4 wt.% Cu.

2.2. Southern Explorer Ridge (SER)

Located approximately 200 km west of Vancouver Island, SER is a moderately fast-spreading ridge with an estimated asymmetrical spreading rate of 7 mm/yr to the east and 21 mm/yr to the west (Botros and Johnson, 1988). It is defined by a single 65 km long, 5–8 km wide segment flanked by deep, flat-floored valleys with an abnormally high standing culmination area (Michael et al., 1989; Scott et al., 1990; Beaudoin, 2007).

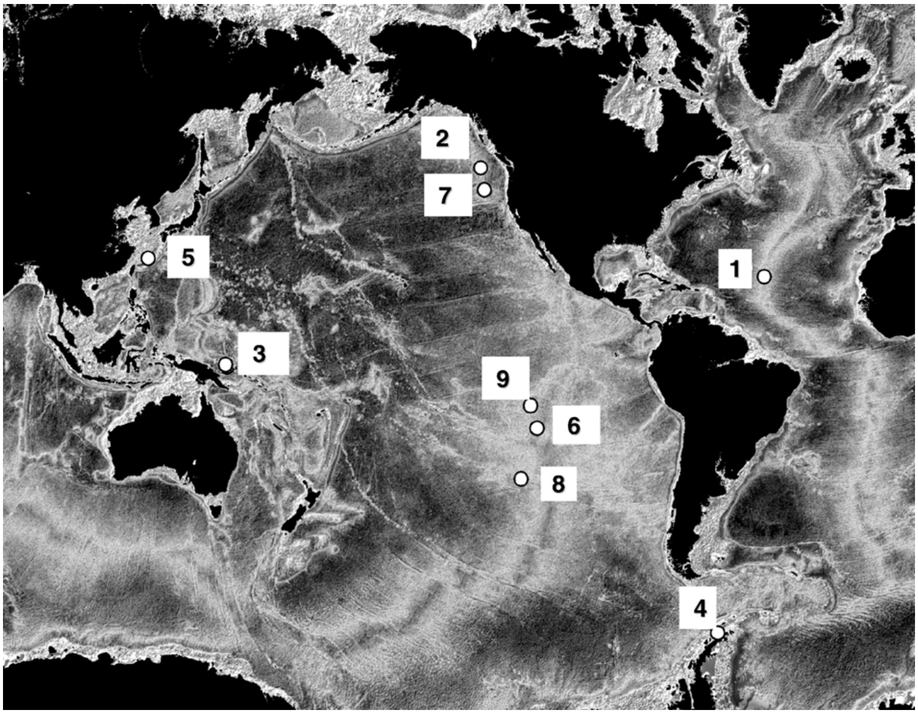

Fig. 1. Study site locations: 1 — mid-Atlantic Ridge; 2 — southern Explorer Ridge; 3 — Manus Basin; 4 — Bransfield Strait; 5 — Okinawa Trough; 6 — Foundation seamount; 7 — Axial seamount; 8 — Pito seamount; 9 — Garrett transform; base map from Walter and Sandwell (1997).

SER was selected for this study as an example of a geochemically atypical mid-ocean ridge. Lava geochemistry ranges from transitional-MORB along the extent of the ridge to enriched-MORB in the vicinity of the culmination. SER basalts are enriched in K, Ti, Rb, Ba, Nb and Zr with respect to normal-MORB (Scott et al., 1990) and show incompatible element ratios characteristic of plume-type mid-ocean ridge magmatism (Erlank and Kable, 1976; Sun et al., 1979). It was proposed by Scott et al. (1990) that the enriched SER basalts originate from a mantle source.

Samples used in this study are basalt recovered during the NOAA 2002 "Submarine Ring of Fire" expeditions in the vicinity of the "Magic Mountain" area of known hydrothermal activity that has resulted in numerous polymetallic sulfide deposits (Scott et al., 1984, 1985; Chase et al., 1986). Hydrothermal deposits consist mainly of Cu–Fe–Zn, Zn–Fe and Cu–Fe sulfide assemblages, Zn–Ba–SiO_2 material as well as metalliferous sediments (Scott et al., 1990). Forty-eight sulfide samples averaged 0.11 wt.% Pb, 5.3 wt.% Zn and 3.2 wt.% Cu.

2.3. Manus back-arc basin: PACMANUS and Susu hydrothermal areas

The Manus Basin is an extensional, oceanic back-arc basin defined by spreading along three segments including the western and central Manus Basin mafic segments, and the eastern Manus Basin mafic-felsic segment (Taylor, 1979; Auzende et al., 1996). To the south is the volcanically active New Britain island arc and its northward dipping trench, which is the current locus of subduction of the Indo-Australian Plate. This current subduction began at approximately 15 Ma, after subduction of the westward moving Pacific plate along the now inactive Manus trench came to a halt upon collision of the Ontong Java plateau (Martinez and Taylor, 1996).

Samples for this study are dacite collected within the eastern Manus Basin and include dredged material from several cruises and drill core from ODP Leg 193. Seafloor extension in this area occurs by pull-apart rifting in remnant island-arc crust and includes volcanic suites of basalt, basaltic andesite, dacite, rhyodacite and rhyolite as evident at the PACMANUS and Susu sites (Binns and Scott, 1993; Scott and Binns, 1995; Moss et al., 1997; Moss et al., 2001; Binns et al., 2002; Shipboard Scientific Party, 2002).

The PACMANUS hydrothermal area is located on an elongated volcanic edifice known as Pual Ridge. Hydrothermal activity is restricted to felsic mounds composed of dacite and rhyodacite overlying a mafic substrate. Compositions of sulfide material in the area include Cu-rich Cu–Zn–Fe–Pb assemblages with minor Au and Ag and Pb–Zn-rich Zn–Pb–Cu–Fe assemblages with trace Au and minor Ag (Binns et al., 1996, 1997). Twenty-six samples averaged 1.7 wt.% Pb, 26.9 wt.% Zn and 10.9 wt.% Cu.

Susu Knolls is located ~40 km east of the PACMANUS field on Tumai Ridge and comprises three distinct venting sites lying atop individual volcanic edifices (Moss et al., 2001). Mounds are composed of dacitic and andesitic lavas. Hydrothermal mineralization at Susu is enriched in Cu and Au and is characterized by stockwork to semi-massive pyrite–fukuchillite–enargite ± covellite–chalcopyrite (Yeats et al., in review). Five samples averaged 0.4 wt.% Pb, 2.1 wt.% Zn and 10.9 wt.% Cu (Moss and Scott, 2001).

2.4. Bransfield Strait marginal basin: Three Sisters and Hook Ridge areas

Bransfield Strait is a marginal basin separating the South Shetland Islands from the west coast of the Antarctic Peninsula. The area is considered to be a back-arc extensional basin characterized by intra-continental rifting (Keller and Fisk, 1992; Keller et al., 1992; Barker and Austin, 1994; Bohrmann et al., 1999). It is in an initial stage of rifting wherein actual seafloor spreading and production of oceanic crust is not occurring (Pelayo and Wiens, 1989; Barker and Austin, 1994; Klepeis and Lawver, 1996). Spreading rate is estimated to be ~1 cm/yr (Dietrich et al., 2001).

The recovered volcanic rocks range in composition from dacite to rhyodacite and exhibit an affinity to typical back-arc basalts (Keller and Fisk, 1992; Lawver et al., 1995; Keller et al., 2002). Felsic volcanic material was also recovered from the Hook Ridge and Three Sisters sites (Keller et al., 2002; Petersen et al., 2004).

Detailed investigations of the water column identified three sites of hydrothermal activity: Hook Ridge, Three Sisters and Little Vulcano (Klinkhammer et al., 1995). Volcanic samples analyzed for this study were collected from, or in the vicinity of, the Hook Ridge and Three Sisters hydrothermal areas.

Located in the northern portion of the Central Bransfield Strait, Hook Ridge is an arched volcanic edifice with a summit that rises to 990 m of water depth. Active hydrothermal sites were located inside a crater on an elongated portion of the ridge (Klinkhammer et al., 2001). Recovered polymetallic sulfides include sulfide–sulfate assemblages enriched in Pb–Ag–As–Sb–Hg, abundant native sulfur and low-Fe sphalerite (Petersen et al., 2004). Seven sulfide samples from Hook Ridge averaged 2.6 wt.% Pb, 18.5 wt.% Zn and 4.5 wt.% Cu (Petersen et al., 2004).

Three Sisters, 75 km southwest of Hook Ridge, consists of three parallel ridges making up a composite volcanic complex with the biggest ridge, Middle Sister, rising to a water depth of 975 m (Petersen et al., 2004). Recovered hydrothermal material from this area consists of two barite–silica samples yielding low concentrations of Fe and other metals although enriched in Au, Ag, Sr, Sb, Tl and Hg relative to Hook Ridge samples (Petersen et al., 2004).

2.5. Central Okinawa Trough continental back-arc: JADE hydrothermal area

The Okinawa Trough is described as an incipient intra-continental back-arc basin formed behind the Ryukyu arc–trench system (Sibuet et al., 1998; Shinjo and Kato, 2000). Geophysical investigations (Hirata, 1991) have determined that the crust in the basin is of continental origin with an increasing thickness from south (~18 km thick) to north (~30 km thick). Within the central Okinawa Trough, geothermal gradients are relatively high encouraging the development of hydrothermal activity, particularly in the IZENA basin (Halbach et al., 1989) that is thought to be a small pull-apart basin (Mann et al., 1983).

The JADE hydrothermal field, located on the northeastern flank of the IZENA basin, is approximately 1000 m long by 200 m wide. Volcanic rocks from the area are of a calc-alkaline, island-arc affinity with a bimodal distribution of basaltic andesite and rhyolite compositions (Halbach et al., 1993). Seventeen samples analyzed from JADE sulfide–sulfate deposits averaged 12.1 wt.% Pb, 24.5 wt.% Zn and 3.1 wt.% Cu. The hydrothermal precipitates exhibit a complex mineralogy involving various assemblages with As, Hg, Ag, and Ba resembling that of Kuroko-type massive sulfides (Halbach et al., 1993; Lüders et al., 2001). Samples used for this study are basalt and one rhyolite (Y129).

2.6. Foundation seamount chain: west of 125° W, intraplate with plume influence; east of 125° W, failed rift propagator

The Foundation seamount chain spans 2000 km of the South Pacific from 33° S 131° W (near the Resolution Fracture Zone) to 37° S 111° W (near the Pacific–Antarctic Ridge) and comprises a series of seamounts and short ridge segments (Mammerickx, 1992; Devey et al., 1996; Hekinian et al., 1997). The chain is inferred to be the surface expression of a mantle plume currently believed to be dying and located about 500 km west of the Pacific–Antarctic Ridge (Hekinian et al., 1999). Samples for this study are basalt collected from two different environments along the Foundation Chain: west of 125° W and between 125° W and 124° W. Volcanic material from areas west of 125° W is basaltic and enriched in incompatible elements representing true intraplate volcanism generated by the Foundation plume whereas material from 125° W to 115° W is andesitic and depleted in incompatible elements and represents lavas from a failed rift propagator of near-ridge origin having little or no plume influence (Devey et al., 1996).

2.7. Axial seamount: ridge–plume interaction

Axial seamount is located on the central Juan de Fuca Ridge at the eastern end of the Cobb-Eickelberg Seamount Chain and is the current expression of the Cobb hotspot (Rhodes et al., 1990). Axial is a 50 km by 70 km shield volcano (at 2600 m of water depth) topped by a 3 km by 7 km, flat floored summit caldera (Hannington and Scott, 1988) at 1500 m water depth. Lava samples for this study are andesitic. Lava chemistries show subtle differences with respect to those of adjoining ridge segments, including higher Na_2O, CaO and Sr contents for a given MgO concentration, indicating that Axial seamount is a discrete volcanic unit with a lava circulation system that is separate from the surrounding ridge system (Rhodes et al., 1990). Though no significant geochemical anomaly is present in Axial volcanic rocks, inferred melting conditions, temperatures and robust supply of magma categorize the hot spot as a thermal anomaly in the mantle as opposed to a geochemically enriched ocean island basalt-type plume (Rhodes et al., 1990).

Hydrothermal activity in the caldera is closely related to recent volcanism and associated eruptive fissures. Sulfide material recovered is generally Zn rich with minor Pb and Cu and significant Au, Ag, As and Sb concentrations (Hannington and Scott, 1988). Fourteen samples averaged 0.35 wt.% Pb, 22.2 wt.% Zn and 0.4 wt.% Cu.

2.8. Pito Seamount, Easter microplate: ridge–plume interaction

Pito seamount is located north of the East Rift propagator on the eastern boundary of the Easter microplate (NW of Easter Island). It lies on a sediment-starved spreading centre that has a full-spreading rate on the order of 5–6 cm/yr (Verati et al., 1999). Volcanic material recovered from Pito seamount includes normal-MORB and enriched-MORB (Hekinian et al., 1996). Hydrothermal activity was first discovered in 1993 (Francheteau et al., 1994) in the form of Zn, Cu and Fe sulfides (Verati et al., 1999). Metal concentrations in the sulfides have not been published.

2.9. Garrett Transform: intra-transform volcanism

The Garrett Transform Fault is one of only two transforms systematically sampled along the fast-spreading southern East Pacific Rise axis (Natland, 1989; Hekinian et al., 1992; Hekinian et al., 1995; Perfit et al., 1996; Niu and Hekinian, 1997; Wendt et al., 1997). Volcanism in the Garrett Transform appears to be restricted to three NE–SW trending ridges along the south wall of the Easter Trough in the East Valley as well as in the southern wall of the Garrett Deep (Wendt et al., 1999). Volcanic material consists mainly of depleted-MORB with low K/Ti, Zr, Ba, Y and Ce/Y (Hekinian et al., 1995). Samples analyzed for this study are basalt collected from flows in the East Trough. No hydrothermal activity has been observed in the Garrett Transform.

3. Methodology

3.1. Sample collection, description, selection and preparation

Samples were collected on various marine expeditions by dredging, occupied submersible dives, unoccupied remotely operated vehicle dives and deep sea core drilling. They included a representative grouping of material recovered from each operation. For this study, 155 separate samples of volcanic rocks were initially examined from 9 different study sites. Altered, heavily weathered and aphyric samples were discarded. Petrological thin sections were cut for 139 phyric samples. Samples lacking melt inclusions were discarded. Large, thick (~100 to 150 μm), doubly polished sections were cut for 75 melt inclusion-bearing samples. Of these, 31 individual samples were selected as the best candidates for analysis (Table 1). No suitable material was recovered from the Three Sisters site in the Bransfield Strait. Volcanic compositions for a given site were limited by sample recovery. Dacite and basaltic andesite samples were available from back-arc environments but only basalt from the remainder.

In general, each selected sample yielded multiple melt inclusion-bearing plagioclase (and a limited number of pyroxene and olivine) crystals that allowed for repeated analyses of the same sample for a total of 108 analyzed inclusions (see Background Dataset,[1] Table 2). Melt

[1] http://www.elsevier.com/locate/margeo.

Table 1
Location, tectonic setting and rock type of samples selected for this study

Field label	Study label	Study site	Local site	Tectonic setting	Rock type
MD-54	MD-54	Eastern Manus Basin	North SuSu Knolls	Immature oceanic back-arc	Fresh dacite
MD-82	MD-82	Eastern Manus Basin	South flank, south Su Knoll	Immature oceanic back-arc	Fresh dacite
MD-83	MD-83	Eastern Manus Basin	South Su Knoll	Immature oceanic back-arc	Fresh dacite
MD-93	MD-93	Eastern Manus Basin	South Su Knoll	Immature oceanic back-arc	Fresh dacite
1189A-010R-1-59	Y36	Eastern Manus Basin	PACMANUS, ODP Leg 193	Immature oceanic back-arc	Moderately altered dacite
SO155-38DR2	Y52	Bransfield Strait	Hook Ridge	Marginal, continental back-arc	Dacite
NBP9904-D18E	Y94	Bransfield Strait	Hook Ridge	Marginal, continental back-arc	Dacite
NBP9904-D17B	Y96	Bransfield Strait	Hook Ridge	Marginal, continental back-arc	Rhyodacite
6K 559-R001	Y129	Central Okinawa Trough	JADE hydrothermal field	Continental back-arc	Fresh rhyollite
6K 562-R008	Y130	Central Okinawa Trough	JADE hydrothermal field	Continental back-arc	Fresh basaltic andesite
6K 562-R010	Y131	Central Okinawa Trough	JADE hydrothermal field	Continental back-arc	Fresh basaltic andesite
6K 562-R011	Y132	Central Okinawa Trough	JADE hydrothermal field	Continental back-arc	Fresh basaltic andesite
6K 569-R002	Y133	Central Okinawa Trough	JADE hydrothermal field	Continental back-arc	Fresh basalt
TN149-R665-RK-0029	Y97	Southern Explorer Ridge	Magic Mountain hydrothermal field	Ridge, with plume influence	Fresh basalt
TN149-R667-RK-1	Y98	Southern Explorer Ridge	Magic Mountain hydrothermal field	Ridge, with plume influence	Fresh basalt
667-RK-01	Y103	Southern Explorer Ridge	Magic Mountain hydrothermal field	Ridge, with plume influence	Weakly altered basalt
Alvin 1676-9	Y114	Mid-Atlantic Ridge	TAG hydrothermal field	Sediment starved ridge	Fresh basalt
Alvin 1679-6	Y120	Mid-Atlantic Ridge	Snakepit hydrothermal field	Sediment starved ridge	Fresh basalt
FH05DR-3B	Y107	Foundation seamount chain	West of 125°W	True intraplate seamount	Alkali basalt
FH07DR-03B	Y113	Foundation seamount chain	Between 125° and 115°W	Failed rift propagator: near ridge origin; little or no plume influence	Basalt
Alvin 2087-5	Y124	Axial seamount		Mantle hot spot interacting with ridge	Fresh basalt
ROP126.9.1 A2	Y126	Axial seamount		Mantle hot spot interacting with ridge	Fresh basalt
Alvin 2087-1	Y137	Axial seamount		Mantle hot spot interacting with ridge	Fresh basalt
Alvin 2087-3	Y138	Axial seamount		Mantle hot spot interacting with ridge	Fresh basalt
Alvin 2087-4	Y139	Axial seamount		Mantle hot spot interacting with ridge	Fresh basalt
PI-07-08	PI-07-08	Pito Seamount	Pito Seamount	Intraplate seamount	Basalt
PI-08-01	PI-08-01	Pito Seamount	Rift Valley, East of Pito Seamount	Intraplate seamount	Basalt
PI-08-02	PI-08-02	Pito Seamount	Rift Valley, East of Pito Seamount	Intraplate seamount	Basalt
GN09-03	GN09-03	Garrett Transform	Median ridge	Transform valley	Picritic basalt
GN09-05	GN09-05	Garrett Transform	Median ridge	Transform valley	Picritic basalt
GN11-09	GN11-04	Garrett Transform	West trough	Transform valley	Basalt

inclusions were selected based on stringent criteria to ensure that all chosen inclusions were fully enclosed. Inclusions with capillaries, fissures or any sign of decrepitation were discarded. Fig. 2 depicts two types of analyzed inclusions: glassy with or without vapor bubble (A, B respectively) and recrystallized (C, D). Diameters ranged from ~10 to 80 μm and were for the most part within ~20 μm of the surface but never directly at the surface. Inclusion-bearing host crystals were broken from the polished thick section and mounted as chips on an 8 mm by 8 mm by 3 mm Vivak™ plate that is optically clear and chemically resistant to acetone and alcohol (Fig. 3). Crystal chips were fixed to the mount using clear nail polish. Quality control documents, Material Safety Data Sheets (MSDS) and analysis by XRF at the University of Toronto ensured no Pb contamination in

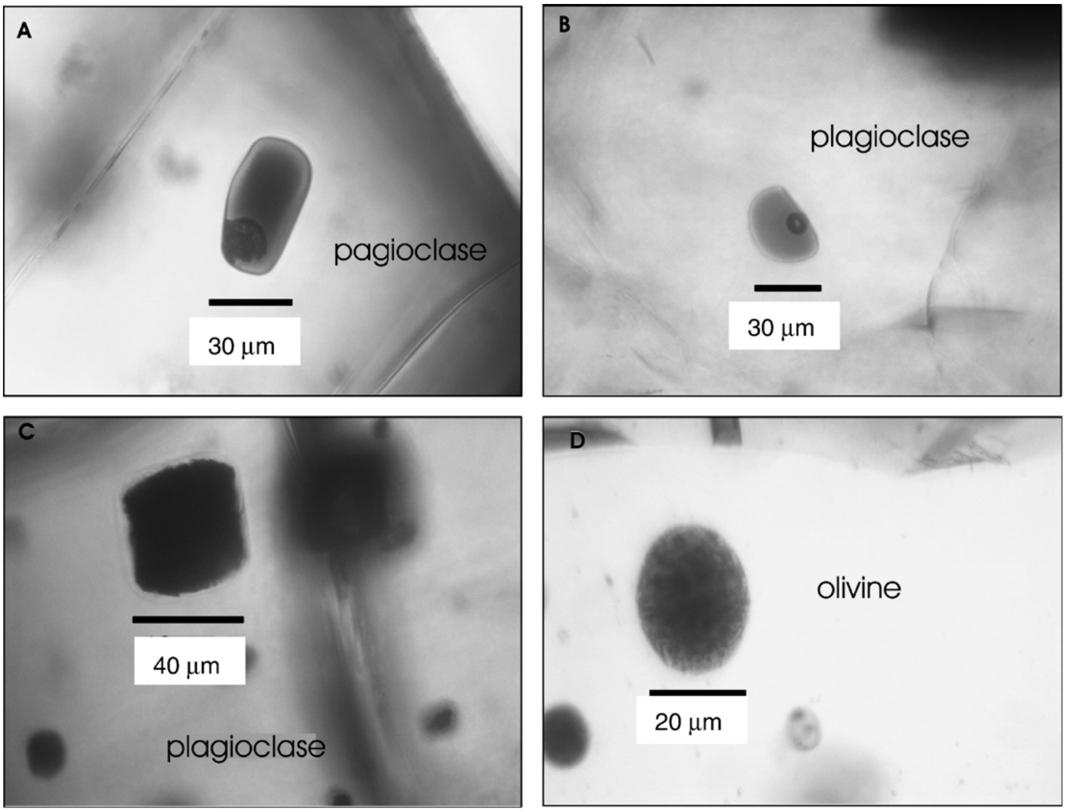

Fig. 2. Example of analyzed melt inclusions. A (Y36-C1-MI1) and B (Y82-C1-MI1) are glassy inclusions with visible vapour/contraction bubble. C (Y107-C1-MI4) and D (Y114-C2-MI1) are recrystallized inclusions.

either the nail polish or mounts. Each mount was washed in acetone and rinsed in isopropyl alcohol prior to analysis to remove surface contamination.

3.2. Compositional variability in host crystal

Microanalyses were performed on host crystals to determine their degree of chemical zonation. Crystals mounted on doubly polished thin sections were analyzed using a Cameca SX50 electron microprobe with three wavelength dispersive spectrometers. Accelerating potential was set at 15 keV, beam current at 10 nA, and a beam size of 15 µm. Na was calibrated against a natural albite; Al and K against a natural sanidine; Ti against synthetic TiO_2; Fe against natural hematite (Elba, Italy); Si, Mn and Ca against natural bustamite; P against natural apatite; and Mg against Kakanui pyrope. Analyses were done as transects from the rim to the core of each crystal with the number of analyses dictated by crystal size. In general, host crystals from a given setting do not show a high degree of variation in An# or Fo# (Fig. 4).

3.3. Laser-ablation ICP-MS

Inclusions were analyzed at ETH Zurich by laser-ablation inductively coupled plasma mass spectrometry

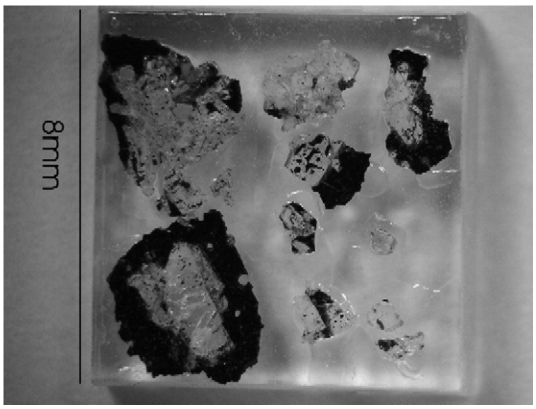

Fig. 3. Example of sample mount (M6) used in the LA-ICP-MS analyses. Mounts are composed of a chemically resistant and optically clear Vivak™ plastic. Sample chips were fixed using a clear nail polish.

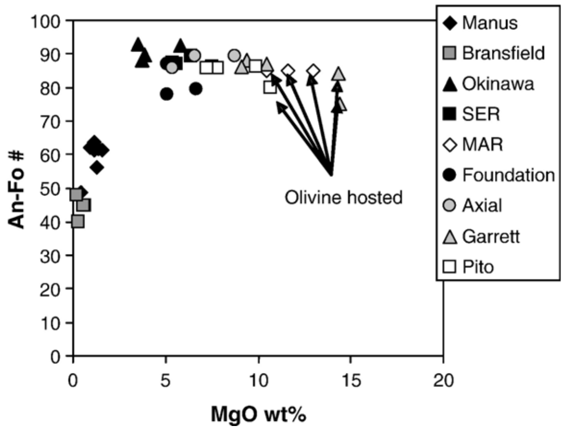

Fig. 4. Host crystal An# and Fo# vs respective melt inclusion MgO; arrows indicate inclusions in olivine host; all other samples are hosted in plagioclase. The analyses demonstrate the homogeneity of the host crystals.

(LA-ICPMS) using a setup developed and described by Günther et al. (1997). The system uses a pulsed 193 nm ArF Excimer laser with a homogenized beam profile. Features include a laterally homogeneous energy distribution that allows for depth-controlled ablation at a rate of 0.1–0.2 μm per shot. Beam size varied in relation to inclusion diameter ranging from approximately 8 to 80 μm and was adjusted to always be slightly larger than the inclusion diameter. One sample block (16 unknowns) at a time was loaded into a 1 cm^3 cell along with a calibration standard. A modified petrographic microscope acts as the experimental stage enabling optical observation and real time control of the ablation process. Ablated aerosol material was carried to an ELAN 6100 quadrupole mass spectrometer by mixed He–Ar carrier gas (Günther and Heinrich, 1999). The ELAN 6100's linear dynamic range of up to nine orders of magnitude in dual detector mode enabled the measurement of 32 elements (for this study) per analysis with concentrations ranging from 100 wt.% to a few tens of ng g^{-1} (Halter et al., 2002). Analyses for selected trace elements including Pb are presented in this paper.

Data were acquired in blocks of 20 analyses with the first and last 2 being analyses of the external standards. For this study, the SRM 610 NIST certified glass (Pearce et al., 1997) was used as the external reference for sensitivity calibrations. A dwell time of 10 ms was used for all elements except for Pb which had a 30 ms dwell time. Measured isotopes were as follows: ^{23}Na, ^{25}Mg, ^{27}Al, ^{29}Si, ^{39}K, ^{42}Ca, ^{45}Sc, ^{49}Ti, ^{52}Cr, ^{55}Mn, ^{57}Fe, ^{65}Cu, ^{66}Zn, ^{75}As, ^{85}Rb, ^{88}Sr, ^{89}Y, ^{90}Zr, ^{93}Nb, ^{137}Ba, ^{139}La, ^{140}Ce, ^{146}Nd, ^{147}Sm, ^{151}Eu, ^{173}Yb, ^{175}Lu, ^{178}Hf, ^{208}Pb, ^{232}Th and ^{238}U. The validity of the technique and the accuracy of the data have been tested in various studies (e.g., Heinrich et al., 2003; Pettke et al., 2004).

3.4. Quantification of LA-ICP-MS data

LA-ICPMS samples the entire melt inclusion enclosed within a host crystal and re-integrates the inclusion's original composition by discriminating between the contribution of the host crystal and that of the inclusion to the overall ablation signal (Halter et al., 2002). The ablation signal (Fig. 5) containing an unknown mix of inclusion and host components can

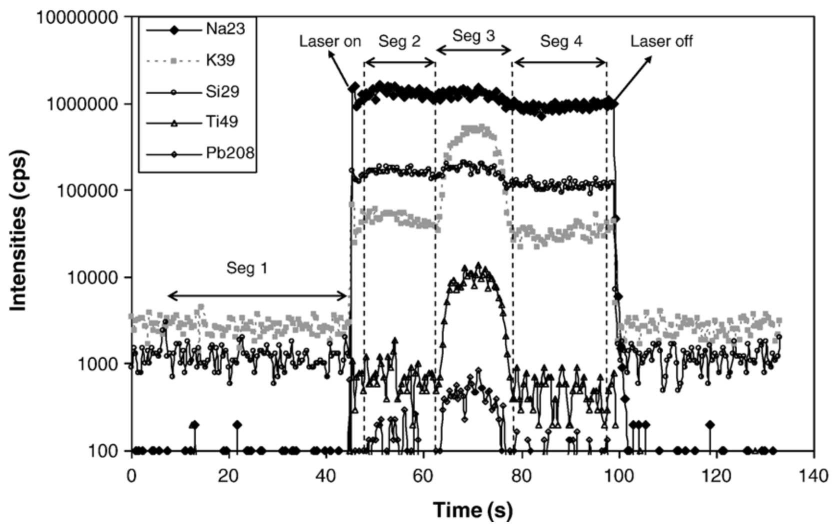

Fig. 5. Example transient signal from the ablation of a plagioclase hosted melt inclusion from eastern Manus Basin. Seg 1: gas background; Seg 2: host crystal ablation; Seg 3: host and melt inclusion ablation; Seg 4: host crystal post inclusion ablation.

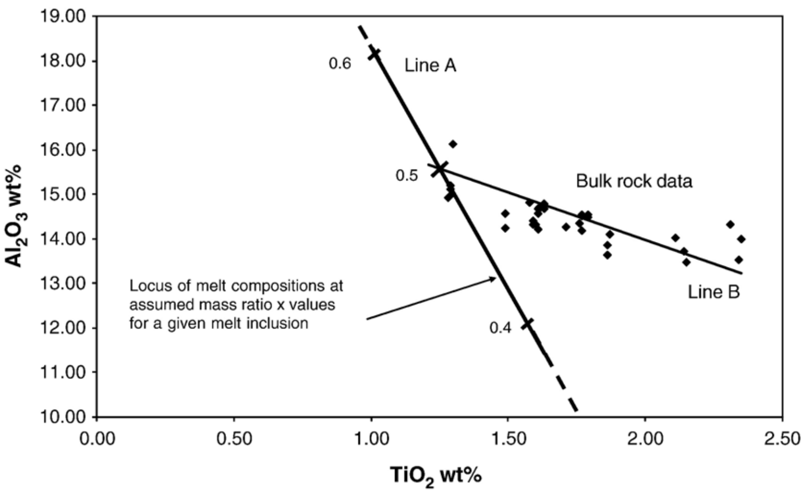

Fig. 6. Quantification of melt inclusion composition by evolution of element ratios in bulk rock differentiation trend. Different, calculated element ratios were obtained by varying the mass ratio of inclusion over total mass ablated in the mixed analysis (line A). The assumption made is that melt inclusions have similar major element ratios (e.g. TiO_2/Al_2O_3) as bulk rocks. This constrains the possible value of the host/inclusion mass ratio which is then used to quantify the concentrations of all other analyzed elements within the inclusions (see text for equations defining the mass ratio x). In this example, for an SER inclusion, at a mass ratio value of 0.5, the inclusion had a TiO_2/Al_2O_3 value that intersected the bulk rock trend (line B, least squares trend line in Excel software). Thus the mass ratio of 0.5 was used to quantify the concentrations of the remaining elements in the inclusion. Adapted from Halter et al. (2004).

be numerically separated into a host contribution and an original trapped melt contribution according to equations derived by Halter et al. (2002). A mass factor x represents the contributing component and is defined as the ratio of the mass of the inclusion over the total ablated mass during the mixed signal interval representing the host crystal and the inclusion (segment 3 in Fig. 5). To obtain the value of this ratio, either the concentration of one element inside the inclusion (internal standard) or the masses of the inclusion and ablated material in the mix, must be determined. Halter et al. (2002) outline 4 different methods for determining the mass ratio. For this study, the internal standard was obtained by using the bulk rock correlation of Ti and Al for all sites. The assumption made is that the correlation of TiO_2 and Al_2O_3, and FeO and Al_2O_3, in whole rocks constrains the concentration of the internal standard element (Al for Garrett, Ti for all others) in the inclusions. Halter et al. (2002) mathematically defines the relationship between x and element concentrations in the inclusions as follows:

$$C_a^{\mathrm{INCL}} = C_a^{\mathrm{HOST}} - \frac{(C_a^{\mathrm{HOST}} - C_a^{\mathrm{MIX}})}{x}$$

and

$$C_b^{\mathrm{INCL}} = C_b^{\mathrm{HOST}} - \frac{(C_b^{\mathrm{HOST}} - C_b^{\mathrm{MIX}})}{x},$$

where C_a^{INCL} is the concentration of TiO_2 and C_b^{INCL} is the concentration of Al_2O_3 in an inclusion.

In a given system, the bulk rock correlation between two elements C_a and C_b can be described by a function f:

$$C_b = f(C_a).$$

Thus for any given x, a value for C_a^{INCL} and C_b^{INCL} is obtained. This calculated trend defines line A in Fig. 6. $C_b = f(C_a)$ of the bulk rock (line B in Fig. 6) constrains the element ratio value for the standard elements in the inclusions. The mass ratio that reflects the element composition, 0.5 in the example in Fig. 6, is then used to quantify the remaining element concentrations in the inclusions.

To exclude a possible artifact due to an inappropriate mass factor, we plotted the compatible element concentrations in the inclusion and the host against each other. On such plots, an uncertainty on the mass factor would generate a trend of the melt inclusion data towards the host composition. Such trends were not observed suggesting that the deconvolution procedure is accurate and not influenced by the host composition. A complete set of analysis of the host minerals is provided in Table A1.

3.5. Boundary layer effects

When using melt inclusions to represent the chemistry of the original melt a host mineral crystallized in, it is assumed that their composition is a true reflection

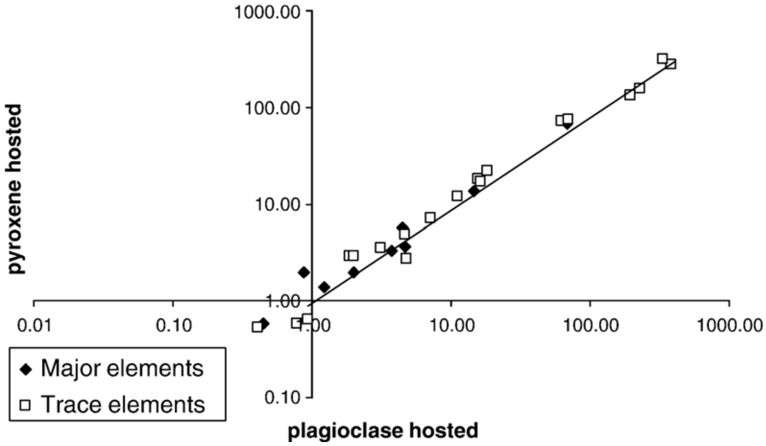

Fig. 7. Composition correlation between melt inclusions hosted in co-existing mineral phases (pyroxene MD83-C1-MI4 and plagioclase MD82-C1-MI4) in the Manus back-arc showing consistency between the hosts. Major elements are in wt.% and trace elements are in ppm. Error bars are 2σ. Line represents 1:1 correlation.

of that melt. Boundary layer effects have been proposed as potential mechanisms that could affect the composition of melt inclusions as the host mineral crystallizes (Lu et al., 1995; Thomas et al., 2002; Kohut and Nielsen, 2004). Host crystal growth rates and mechanisms are key factors in the trapping of primary inclusions that represent the composition of a melt at the time of entrapment. Kohut and Nielsen (2004), in experiments where plagioclase crystals were formed in a silicate melt at various cooling rates (from 1300 °C to 1210 °C with 1–10°/min cooling rates followed by 0–116 h isothermal periods), determined that with isothermal times and cooling rates most favorable to melt inclusions formation (24 h<6 h and 5°/min respectively), a boundary layer was not entrapped and no compositional effect on the inclusions was detected. With respect to all experiments, only inclusions formed during slow cooling (1°/min) showed slight compositional diversity. Work done on the latter to detect rejected components expected to be found in an entrapped boundary layer (TiO_2 as a rejected species in plagioclase hosted inclusions) yielded no systematic increase in rejected components with decreasing inclusion size. An increase would be anticipated as the smaller inclusions would contain proportionately more of the boundary layer. Halter et al. (2004) also plotted melt inclusion compositions against size with the idea that an entrapped boundary layer should have a larger effect on small inclusions resulting in a correlation between the size and the composition if the boundary layer effect is important. No correlation was observed. Halter et al. (2004), using LA-ICP-MS, compared analytical results from a lava suite that hosted melt inclusions in co-existing mineral pairs (e.g. pyroxene–plagioclase, plagioclase–amphibole). Melt inclusion compositions were consistent between the contrasting mineral hosts indicating an absence of a boundary layer effect.

The expected effects of boundary layer entrapment would be different from one mineral host to another as the species rejected from the melt inclusions would vary (e.g. TiO_2 for plagioclase hosts and CaO for pyroxene hosts) resulting in differing compositional variability. Fig. 7 demonstrates the compositional consistency between two melt inclusions from the Manus back-arc hosted in co-existing mineral phases (plagioclase and pyroxene) and analyzed for this study. Thomas et al. (2002) obtained similar results using electron microprobe analyses of melt inclusions hosted in various co-genetic mineral phases from the Toba Tuff. The misfits in Fig. 7 are MgO, Cu and, to a lesser extent, Ba and Sr. Mg can diffuse in pyroxene (Halter et al., 2004). Cu can be enriched in plagioclase-hosted inclusions due to heterogeneous entrapment of a volatile phase (Yang and Scott, 2006; Zajacz and Halter, 2007). The low Ba and Sr could be a consequence of a slight difference in the composition of the plagioclase subtracted from the mixed signal and the actual plagioclase around the inclusion.

4. Results: Pb, Cu and Zn in melt inclusions

Fig. 8A contains the Pb values for all analyzed melt inclusions. Back-arc settings as a whole have the highest Pb values (highest observed was 27.4 ppm at Okinawa; sample of rhyolitic affinity) whereas seamounts and Garrett transform have the lowest (0.1 ppm at Pito and Foundation seamounts is the lowest value). All mid-ocean ridges and seamounts exhibit low Pb variability for a given site. At back-arc sites, ΔPb (the variation of Pb within the melt inclusion population) ranges from about 3.5 ppm at Manus (basaltic andesite, plagioclase + clinopyroxene assemblage) and 7.7 ppm at Bransfield (dacite, plagioclase-only assemblage) to a notable 26 ppm for a highly fractionated rhyolite, plagioclase-only assemblage (Y129) at Okinawa; ~3 ppm for the other Okinawa samples.

Cu concentrations in melt inclusions show important variability among the 3 back-arc settings (Fig. 8B). Manus dacitic samples are the most Cu-rich (up to 3690 ppm) and are enriched with respect to bulk rock and MORB. Okinawa basaltic samples have Cu values up to 259 ppm with ΔCu of 75 ppm and are also enriched with respect to bulk rock and MORB. Bransfield rhyodacite and dacite samples are a notable exception with relatively low Cu (3 to 33 ppm

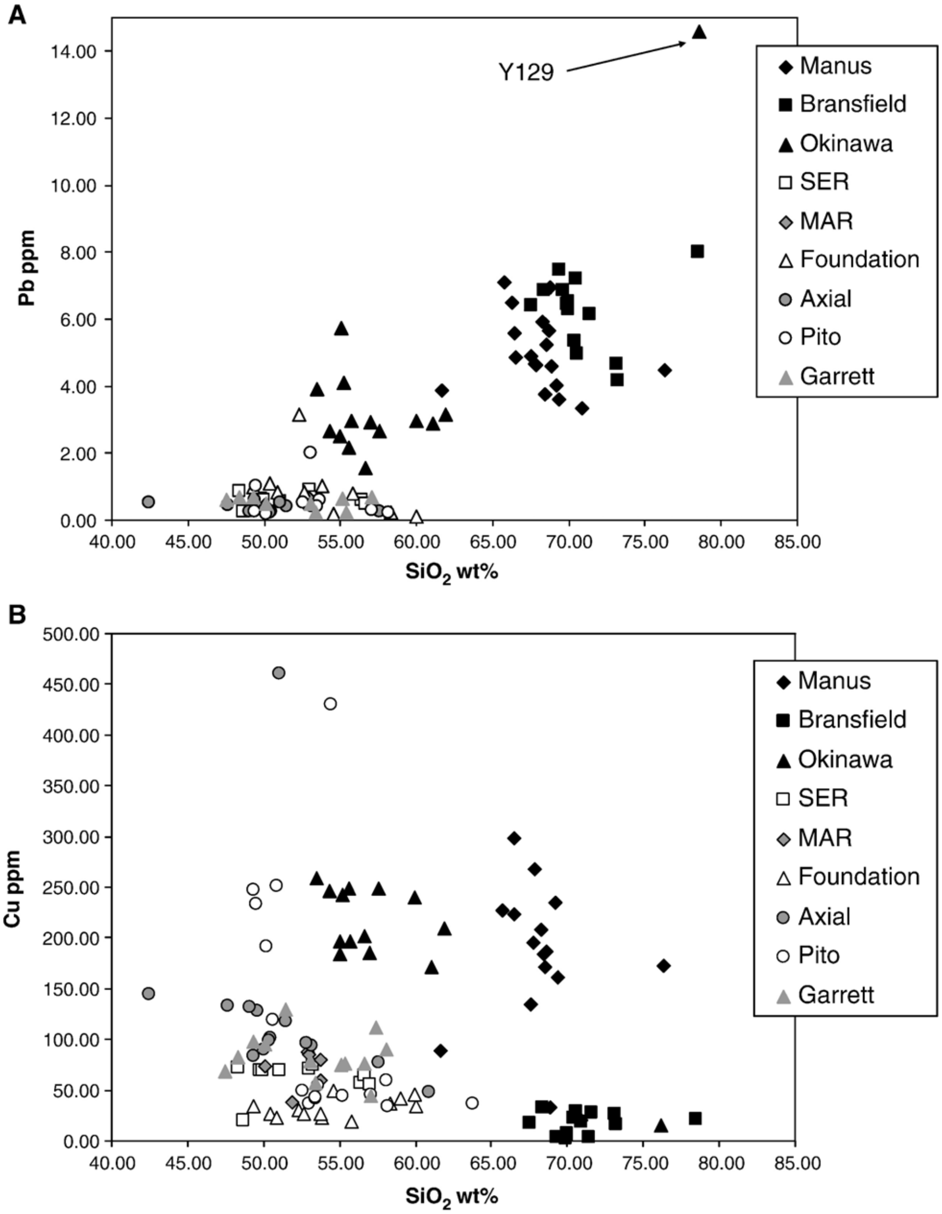

Fig. 8. Metals vs SiO_2 in melt inclusions showing the lack of systematic variability with crustal setting. (A) Pb increases with silica content, Y129 is a highly fractionated rhyolite from Okinawa. (B) Cu displays significant variability among the back arcs but not in the other settings. (C) Zn variability is not large among the sites.

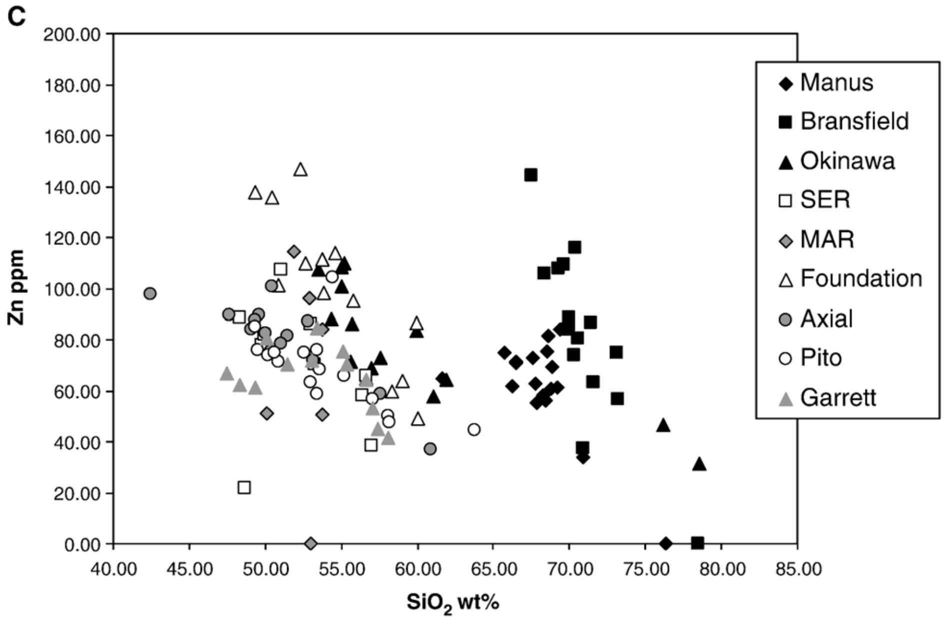

Fig. 8 (*continued*).

respectively). Cu values in inclusions from other tectonic settings are not highly variable even between settings (Fig. 8B). Both SER and MAR have Cu concentrations in the MORB range. Notable exceptions include high Cu values in olivine-hosted inclusions compared to plagioclase-hosted inclusions from Pito and in 6 Axial samples with >100 ppm Cu (1 sample with 460 ppm Cu). Inclusions from Pito and Foundation (near-ridge population, sample Y113) have Cu values similar to MORB.

Zn values do not vary greatly among study sites (Fig. 8C). Including outliers, ΔZn is 108 ppm between the lowest concentration (37 ppm at Axial) and the highest (145 ppm at Bransfield). Excluding the few outliers, ΔZn is only about 50 ppm over the range of data. Foundation samples from the plume-influenced volcanic province have the highest systematic Zn values (from 95 to 138 ppm).

In summary, relative to MORB (Hofmann, 1988), Manus inclusions (dacite hosted with some rhyodacite hosted) are enriched in Cu, have similar Zn concentrations and are enriched in Pb; Bransfield inclusions (dacite hosted) have depleted Cu values, have similar Zn values and are enriched in Pb; Okinawa inclusions (basalt, basaltic andesite and rhyolite-hosted) are enriched in Cu, are slightly enriched in Zn and are enriched in Pb.

In the mid-ocean ridge setting, SER (basalt-hosted) has similar Cu and Zn values and is overall slightly enriched in Pb with respect to N-MORB; Axial (basalt-hosted) is slightly enriched in Cu, has similar Zn values and has similar to slightly depleted Pb values; near-ridge Foundation samples (basalt-hosted) are depleted in Cu, Zn and Pb.

Relative to primitive mantle (McDonough and Sun, 1995), Foundation intraplate inclusions have similar to slightly depleted Cu values and are enriched in Zn and Pb. Garrett inclusions (picritic basalt-hosted) are enriched in Cu and Zn and slightly enriched in Pb.

Variability in the composition of melt inclusions has been observed in previous studies. Danyushevsky et al.

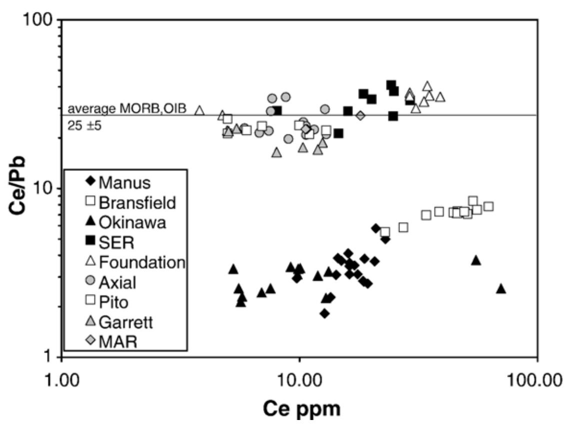

Fig. 9. Ce/Pb vs Ce diagram. Average MORB and OIB Ce/Pb value is indicated (25±5). Note the lower Ce/Pb ratio in arc and back-arc settings.

(2004) pointed out that melt inclusions in primitive mantle-derived magmatic rocks (Fo > ~85 mol%) at mid-ocean ridges and subduction zones can have anomalous compositions as a consequence of processes taking place at the margin of a magma body. Very little information is available regarding possible effects of post entrapment processes, such as re-equilibration by diffusion, with respect to Pb in melt inclusions hosted in plagioclase. Michael et al. (2002) noted that a small percentage of melt inclusions in plagioclase from a mid-Atlantic ridge N-MORB exhibited strong depletion of high field strength element (e.g. Zr, Ti, Nb) with respect to the host glass. REE were moderately depleted and LILE (including Pb) were not depleted. Two scenarios were proposed to explain this post entrapment effect on HFSE: 1 — rapid dissolution of plagioclase yielded a plagioclase-rich melt into which incompatible elements diffused into the inclusion from the host; diffusion could occur through melt channels assuming very rapid conditions or through solid plagioclase under very slow conditions. 2 — HFSE-depleted inclusions could form by trapping ultra-depleted melt inclusions followed by diffusion of incompatible elements from a later, more enriched host melt through solid plagioclase. The important observation to note is that Pb depletion between the host glass and the HFSE-depleted melt inclusions was not observed indicating that, even under partial plagioclase dissolution, Pb is apparently not removed from the inclusion.

5. Discussion

Previous studies on melt inclusions have focused on the diversity, origins and evolution of magmas from numerous modern seafloor sites. This study expands on the earlier work by examining budgets of Pb and other ore metals in back-arc basins, mid-ocean ridge and seamount magmas for the insights each can provide regarding the concentration of Pb in parental magmas.

5.1. Back-arcs

Fig. 9 is a Ce/Pb vs Ce plot that discriminates between the MORB/OIB and arc related sources. The premise is that Ce and Pb, elements with similar solid-melt distribution coefficients, behave similarly during mantle melting (Miller et al., 1994). The preferential enrichment of Pb over Ce in arc and back-arc settings is the result of non-magmatic processes related to the subduction of oceanic crust (and associated sediments). All three back-arcs from this study clearly reflect the enrichment in Pb and its effect on the Ce/Pb ratio. Similarly, Bransfield melts exhibit higher La/Pb ratios for a given SiO_2 content (see Background Dataset,[2] Table 2). As was the case for Ce and Pb, this ratio remains relatively unfractionated during crystallization due to similar melt partitioning of both elements. Thus the difference indicates the influence of a non-magmatic process. The observed increase in the La/Pb ratio at Bransfield would support the idea of pre- or syn-erruptive loss of Pb.

The apparent distinctiveness between Bransfield and Manus inclusions (considering similar volcanic compositions) may reflect a fundamental difference in the subduction processes at these sites. Dehydration of a subducted slab is known to transfer fluid-mobile elements and volatiles into the source regions of arc and back-arc magmas (e.g. Brenan et al., 1995). Bransfield inclusions are depleted in fluid-mobile elements such as As, K and Ba, have higher Ce/Pb (Fig. 9) and U/Th ratios than Manus and the lavas are volatile poor ($H_2O < 1$ wt.% (Keller et al., 2002) vs 2–4 wt.% (Yang and Scott, 1996) and < 2 wt.% (Kamenetsky et al., 2001) at Manus). This would suggest a reduced contribution of slab-derived fluids in the magma source of the Bransfield back-arc. Perhaps there was an early degassing at Bransfield that carried away the Cu.

Zn and Pb concentrations in Bransfield inclusions are similar to those found at Manus whereas Cu averages ~13 ppm compared with ~200 ppm at Manus (for the same SiO_2 value). Cu values at Bransfield are depleted with respect to MORB whereas the Manus melts are actually enriched in Cu with respect to MORB. For subduction settings, in addition to mobilizing various trace elements including Pb and Zn, it has been suggested that slab-derived fluids may also transfer Cu from the dehydrating slab (Stolper and Newman, 1994; de Hoog et al., 2001). Regardless of the Cu content of the subducted slab, if the process of element transfer from the slab to the mantle wedge is inefficient or not occurring (as suggested by low fluid mobile element concentrations in melts from Bransfield), it would indicate that Pb and Zn at Bransfield have a different origin to that of Cu. Bransfield being a back-arc basin occurring on a continental margin, it is possible that contamination by the addition of continental crust may be the main source for Pb and Zn. However, this does not explain the similarity in Pb and Zn contents of melt inclusions between Bransfield and Manus when there is no continental crust at Manus.

Alternatively, the low concentrations of Cu at Bransfield relative to Manus may reflect geochemical conditions in the mantle source (at Bransfield) that

[2] Please see Footnote 1.

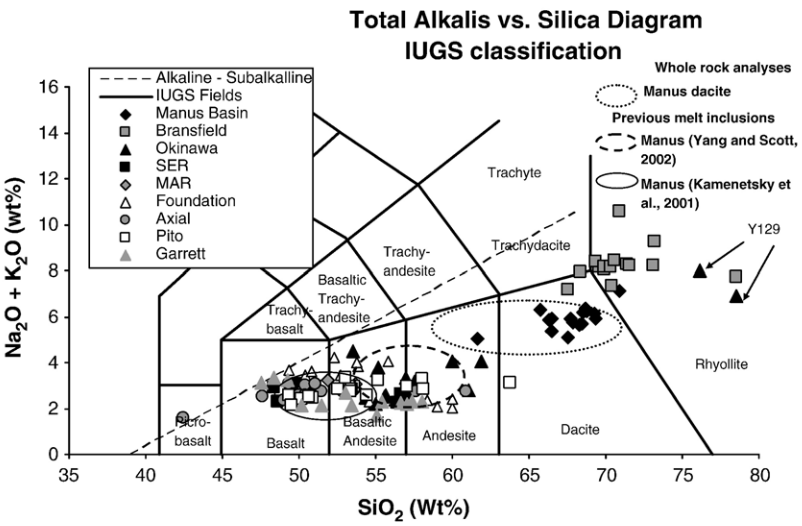

Fig. 10. Total alkalis vs silica in melt inclusions for the IUGS classification. Ranges of whole rock compositions are similar to those of their melt inclusions. The whole rock analyses for Manus dacite are from Yang and Scott (2002), Moss et al. (2001), and Yeats et al. (in review).

inhibit the availability of chalcophile elements in back-arc magmas. Mungall (2002) suggests that the presence of immiscible sulfide melt in the magma source sequesters Cu during partial melting of the mantle resulting in Cu poor magmas (like those at Bransfield). This does not necessarily mean that sulfide melts must be absent from the mantle source in order for a silicate magma to contain significant amounts of Cu. According to de Hoog et al. (2001), the Cu concentration of a primary melt is a function of sulfur solubility in the melt, which is strongly dependent on the oxidation state of the magma, and on S and Cu in the mantle source. Ferric iron, added to the melt source via slab-derived fluxing, could lead to the production of sulfide-undersaturated magmas that are rich in Cu. Ferric iron fluxing into the mantle in a subduction setting would involve the production of slab melts acting as transfer agents and suggests possible tectonic controls that involve a high temperature, low pressure path for the subducting slab (e.g. flat subduction, stalled subduction) (Mungall, 2002). However, because sulfur solubility in a magma is so very pressure-dependent (e.g., Mavrogones and O'Neill, 1999), the source may contain residual (Cu-rich) sulfide even though magmas are sulfur-undersaturated at shallow levels and sulfides are not observed.

Okinawa inclusions of basaltic–andesitic to rhyolitic affinities lie on the same evolution trend as the Manus dacitic inclusions (Fig. 10). Both magmatic regimes are rich in volatiles (H_2O=<2–4 wt.%) and are highly phyric with >20% plagioclase, pyroxene and rare olivine in analyzed samples. Both are generally enriched in fluid-mobile elements although Manus has distinctly more elevated K/La and U/Th ratios. Ce/Pb, Cu and Zn values are similar for both sites. The eastern Manus basin setting is dominated by older arc crust. With a trace element chemistry supporting a subducted slab-derived contribution, the source of Pb, Cu and Zn is likely linked to the slab dehydration process.

5.2. Magma enrichment at ridges and intraplate seamounts

Magmas at ridges can undergo enrichment under the influence of mantle plumes that contribute material to the MORB source (e.g., Hekinian et al., 1999). Enriched lavas from intraplate environments such as seamounts are potentially the result of mantle plume-related contamination (e.g., Hekinian et al., 2004) or of recycling of subducted oceanic crust (Hofmann et al., 1986; Niu and Batiza, 1997). Contamination from either source may be an important component of ore metal budgets, particularly Pb, in these settings.

SER and Axial both lie on the same mid-ocean ridge system off the west coast of North America. Axial is described as a slightly off-axis seamount while SER morphologically resembles an on-axis seamount. Both have active polymetallic sulfide- precipitating hydrothermal systems dominated by Cu and Zn. Basalt-hosted melt inclusion compositions differ significantly suggesting two distinct magmatic regimes despite similar ridge–seamount morphology. SER inclusions are characterized as highly enriched-MORB according to the criteria of incompatible element ratios defined by Niedermann et al. (1997). With K/Ti>0.3 and $(Ce/Yb)_n$>2.5, SER melt inclusions are clearly recording a contribution to the MORB source of a component geochemically consistent with mantle plume material. SER melts are also highly enriched in Ba, Nb and Ce with respect both to MORB and to Axial inclusions. At Axial, the K/Ti ratios of melt inclusions range between 0.11 and 0.18 (one exception at 0.45) and $(Ce/Yb)_n$ ratios are generally between 1 and 1.5 defining the melts as transitional-MORB. No highly enriched-MORB has been observed at Axial whereas, at SER, the ridge length is characterized by enriched- (mainly in the area of the bathymetric minimum), transitional- and normal-MORB (furthest away from the bathymetric minimum). No significant off axis volcanic constructions are present at SER whereas Axial is at the eastern end of the Cobb–Eickelberg Seamount chain and represents the current center of the Cobb Hotspot. The composition of melt inclusions from Axial supports the model proposed by Rhodes et al. (1990) in which the Cobb-Eickelberg Seamount chain and Axial seamount represent a thermal anomaly in the mantle. At SER, the ridge did not migrate over a pre-existing plume. The physiology of the ridge and composition of the melt inclusions are consistent with a sustained contribution of mantle plume material enriching the melt with respect to MORB and increasing the overall magma budget of the site. With respect to metal budgets, concentrations of Cu, Zn and Pb in inclusions from either site do not vary significantly from MORB values. This seems to indicate that, despite the addition of enriched material at SER, metal budgets in the parental magmas of each site are dominated by the original MORB source.

At TAG on the mid-Atlantic ridge, Pb values range between 0.5 and 0.7 ppm (MORB range) while inclusions from the Snakepit hydrothermal field have Pb concentrations that are below detection limit (<0.87 ppm). Inclusions from both sites were from olivine hosted in basalt.

In the Foundation seamount system, an enriched source signature is clearly evident for inclusions hosted in a lava from west of 125° W (intraplate seamount; Y107) erupted along an elongated edifice characterized by three volcanic cones. Inclusions in this alkali basalt with K/Ti > 0.30, and $(Ce/Yb)_n = 3–6.5$ are distinct from those analyzed in a sample (Y113) from a failed rift propagator (near-ridge type regime) which have K/Ti = 0.11–0.15 and $(Ce/Yb)_n = 0.55–0.90$ consistent with more typical MORB characteristics. The two previous samples represent a time (>20 Ma) when the Foundation hotspot was actively building seamount edifices in proximity to a spreading regime that failed to mature. The two distinct melt inclusion compositions clearly indicate the independence of the near ridge environment from the intraplate Foundation source. Zn and Pb concentrations between the two environments are affected by the addition of enriched material (from mantle upwelling or recycled oceanic crust), in contrast to SER and Axial. In fact, the Foundation intraplate inclusions are more enriched in Zn and slightly more enriched in Pb than at SER and Axial but are slightly depleted in Cu. This supports the previous suggestion that, in an on-axial or near-axial setting, the addition of enriched material from a plume or recycled oceanic crust source is not the critical factor controlling the concentration of ore metals in the underlying parental magmas as it is in off-axis or intraplate settings.

Pb isotopes at Pito Seamount (Verati et al., 1999) suggest that the source of Pb in local hydrothermal deposits may be related to a “past local mantle anomaly” underlying the seamount. Melt inclusion chemistry strongly supports the addition of enriched material. Inclusions have T-MORB characteristics with K/Ti = 0.18–0.30 and $(Ce/Yb)_n = 0.65–1.83$. One sample (PI0802) contains melt inclusions with N-MORB affinities. As a whole Cu, Zn and Pb budgets once again appear to be unrelated to possible contamination from a mantle plume or recycled oceanic crust as concentrations of the metals overlap that of uncontaminated and enriched melts.

6. Conclusions

Melt inclusions of the 9 examined study sites provide important insights into the relationships between magmatic history and concentrations of ore metals, with a particular focus on Pb. For the back-arc environments, inclusions demonstrate the influence of subduction-related processes such as slab-dehydration and the transfer of elements into the parental magma source.

For non back-arc settings, contamination from an enriched source plays a distinct role in metal concentrations in melt inclusions depending on tectonic setting. Near or at mid-ocean ridge seamounts display very little relationship between Zn and Pb concentrations and the source of parental melts while in true intraplate settings, the input of enriched material plays a key role. Cu values appear to be independent of the enrichment process as concentrations do not vary between spatially close intraplate and near-ridge settings.

Determining the availability of Pb in the parent magmas of seafloor hydrothermal systems is the first step in evaluating the potential of direct metal contribution by magmatic degassing. Back-arcs as a whole have the most Pb-rich sulfide deposits on the seafloor relative to other tectonic settings. The current work shows that these Pb-rich sulfide systems are associated with Pb-enriched magmas relative to those from non-back arc settings. It would appear that there is a correlation between the Pb concentrations in the parent magmas as observed in melt inclusion data, the potential for magmatic degassing of metals and the final concentration of Pb in the hydrothermal precipitates.

Acknowledgments

We gratefully acknowledge sample contributions from Brian Cousens (Carleton University), Yves Fouquet (IFREMER), Kathy Gillis (University of Victoria), Roger Hekinian (IFREMER), Susan Humphris (WHOI), Randy Keller (Oregon State University) and Michael Perfit (University of Florida). Insightful discussion with Kaihui Yang (University of Toronto) contributed to the development and progress of the study. Beaudoin thanks the science parties and ship crews of the following campaigns on which he participated: SO-155 (Bransfield) and SO-167 (Louisville–Tonga) aboard R/V Sonne, Manaute 2000 aboard R/V L'Atalante and Submarine Ring of Fire Leg 1 (SER) aboard R/V Thomas. G. Thompson. Two anonymous reviews were very helpful. This project was funded by NSERC grants to Scott and SEG grants to Beaudoin.

Appendix A. Supplementary data

Supplementary data associated with this article can be found, in the online version, at doi:10.1016/j.margeo.2007.04.004.

References

Auzende, J.-M., Urabe, T., Scientific Party of the ManusFlux Cruise, 1996. Submersible observation of tectonic, magmatic and hydrothermal activity in the Manus Basin (Papua New Guinea). EOS Trans. Am. Geophys. Union, WPMG Supplement 77, W115.

Barker, D.H.N., Austin Jr., J.A., 1994. Crustal diapirism in Bransfield Strait, West Antarctica; evidence for distributed extension in marginal-basin formation. Geology (Boulder) 22, 657–660.

Beaudoin, Y., 2007. Developing a seafloor GIS for the southern Explorer Ridge hydrothermal site: 2D, 2.5D and dynamic modeling applications. In: Berdusco, B.H., Wright, J. (Eds.), GIS Applications in the Earth Sciences. Geol. Assoc. Can. Monogr. 44, 451–468.

Binns, R.A., Scott, S.D., 1993. Actively forming polymetallic sulfide deposits associated with felsic volcanic rocks in the eastern Manus back-arc basin, Papua New Guinea. Econ. Geol. Bull. Soc. Econ. Geol. 88, 2222–2232.

Binns, R., Waters, J.C., Carr, G.R., Whitford, D.J., 1996. A submarine andesite–rhyodacite lineage of arc affinity, Pual Ridge, eastern Manus back-arc basin, Papua New Guinea. EOS Trans. Am. Geophys. Union 77, W119–W120.

Binns, R., Scott, S.D., Gemmell, J.B., Crook, K.A.W., 1997. The Susu Knolls hydrothermal field, eastern Manus basin, Papua New Guinea. EOS Trans. Am. Geophys. Union 78, F772.

Binns, R.A., Barriga, F.J.A.S., Miller, D.J., Scientific Party, 2002. Proceedings of the Ocean Drilling Program, Initial Reports; Anatomy of an Active Felsic-hosted Hydrothermal System, Eastern Manus Basin; Covering Leg 193 of the Cruises of the Drilling Vessel JOIDES Resolution; Apra Harbor, Guam, to Townsville, Australia; sites 1188–1191, 7 November 2000–3 January 2001 Proceedings of the Ocean Drilling Program, Part A: Initial Reports, vol. 193. variously paginated.

Bogdanov, Y.A., Gurvich, E.G., Lisitsyn, A.P., Muraviov, K.G., Isaeva, A.B., Ivanov, G.V., Krasnyuk, A.D., 1995. A newly discovered relict hydrothermal mound in the TAG hydrothermal field, Mid-Atlantic Ridge, 26°N. Ridge Newsl. 8, 16–19.

Bohrmann, G., Chin, C., Peterson, S., Sahling, H., Schwarz-Schampera, U., Greinert, J., Lammers, S., Rehder, G., Daehlmann, A., Wallmann, K., Dijkstra, S., Schenke, H.W., 1999. Hydrothermal activity at Hook Ridge in the Central Bransfield Basin, Antarctica. Geo Mar. Lett. 18, 277–284.

Botros, M., Johnson, H.P., 1988. Tectonic evolution of the Explorer—Northern Juan de Fuca region from 8 Ma to the present. J. Geophys. Res., B 93, 10421–10437.

Brenan, J.M., Shaw, H.F., Ryerson, F.J., 1995. Experimental evidence for the origin of lead enrichment in convergent-margin magmas. Nature (London) 378, 54–56.

Chase, R.L., Scott, S.D., McConachy, T.J., Barrett, T.J., Gorton, M.P., Denton, A.W.S., Shea, G.T.F., Fouquet, Y., Kawahata, H., McMillan, W.J., Wolfe, W.J., Lichtblau, A.P., Alton, M., Criswick, J., Michael, P.J., 1986. Hydrothermal activity discovered on northern Explorer Ridge; sulphides dredged on southern Explorer Ridge; results of CASM 6 Expedition, N.E. Pacific Ocean. In: Anonymous (Ed.), AGU 1986 Fall Meeting and ASLO Winter Meeting EOS Trans. Am. Geophys. Union, p. 1283.

Danyushevsky, L.V., Leslie, R.A.J., Crawford, A.J., Durance, P., 2004. Melt inclusions in primitive olivine phenocrysts: the role of localized reaction processes in the origin of anomalous compositions. J. Petrol. 54, 2531–2553.

de Hoog, J.C.M., Mason, P.R.D., van Bergen, M.J., 2001. Sulfur and chalcophile elements in subduction zones; constraints from a laser ablation ICP-MS study of melt inclusions from Galunggung Volcano, Indonesia. Geochim. Cosmochim. Acta 65, 3147–3164.

Devey, C.W., Hekinian, R., Ackermand, D., Binard, N., Francke, B., Hemond, C., Kapsimalis, V., Lorenc, S., Maia, M., Moeller, H., Perrot, K., Pracht, J., Rogers, T., Stattegger, K., Steinke, S., Victor, P., 1996. The Foundation Seamount Chain; a first survey and sampling. Mar. Geol. 137, 191–200.

Dietrich, R., Dach, R., Engelhardt, G., Ihde, J., Korth, W., Kutterer, H.-J., Lindner, K., Mayer, M., Menge, F., Miller, H., Müller, C., Niemeier, W., Perlt, J., Pohl, M., Salbach, H., Schenke, H.W., Schoene, T., Seeber, G., Veit, A., Volksen, C., 2001. ITRF coordinates and plate velocities from repeated GPS campaigns in Antarctica — an analysis based on different individual solutions. J. Geodyn. 74, 756–766.

Erlank, A.J., Kable, E.J.D., 1976. The significance of incompatible elements in mid-Atlantic Ridge basalts from 45°N with particular reference to Zr/Nb. Earth Planet. Sci. Lett. 54, 281–291.

Fouquet, Y., Wafik, A., Cambon, P., Mevel, C., Meyer, G., Gente, P., 1993. Tectonic setting and mineralogical and geochemical zonation in the Snake Pit sulfide deposit (Mid-Atlantic Ridge at 23°N). Econ. Geol. Bull. Soc. Econ. Geol. 88, 2018–2036.

Francheteau, J., Naar, D.F., Scientific Party, 1994. Black smokers discovered, Pito Seamount, near Easter microplate propagator tip. AGU 1994 Spring Meeting EOS Trans. Am. Geophys. Union, p. 322.

Günther, D., Heinrich, C.A., 1999. Enhanced sensitvity in laser ablation-ICP- mass spectrometry using helium–argon mixtures as aerosol carrier. J. Anal. At. Spectrom. 14, 1363–1368.

Günther, D., Frischknecht, R., Heinrich, C.A., Kahlert, H.J., 1997. Capabilities of an Argon Fluoride 193 nm Excimer Laser for Laser Ablation Inductively Coupled Plasma Mass Spectrometry Microanalysis of Geological Materials. J. Anal. At. Spectrom. 12, 939–944.

Halbach, P., Nakamura, K., Washner, M., Lange, J., Sakai, H., Käselitz, L., Hansen, R.-D., Yamano, M., Post, J., Prause, B., Seifert, R., Michaelis, W., Teichmann, F., Kinoshita, M., Märten, A., Ishibashi, J., Czervinski, S., Blum, N., 1989. Probable modern analogue of Kuroko-type massive sulfide deposits in the Okinawa Trough back-arc basin. Nature (London) 338, 496–499.

Halbach, P., Pracejus, B., Märten, A., 1993. Geology and mineralogy of massive sulfide ores from the Central Okinawa Trough, Japan. Econ. Geol. Bull. Soc. Econ. Geol. 88, 2210–2235.

Halter, W.E., Pettke, T., Heinrich, C.A., Rothen-Rutishauser, B., 2002. Major to trace element analysis of melt inclusions by laser-ablation ICP-MS: methods of quantification. Chem. Geol. 183, 63–86.

Halter, W.E., Pettke, T., Heindrich, C.A., 2004. Laser-ablation ICP-MS analysis of silicate and sulfide melt inclusions in an andesitic complex I: analytical approach and data evaluation. Contrib. Mineral. Petrol. 147, 385–396.

Hannington, M.D., Scott, S.D., 1988. Mineralogy and geochemistry of a hydrothermal silica–sulfide–sulfate spire in the caldera of Axial seamount, Juan de Fuca Ridge. Can. Mineral. 26, 603–625.

Heinrich, C.A., Pettke, T., Halter, W.E., Aigner-Torres, M., Audétat, A., Günther, D., Hattendorf, B., Bleiner, D., Guillong, M., Horn, I., 2003. Quantitative multi-element analysis of minerals, fluid and melt inclusions by laser-ablation inductively-coupled-plasma mass spectrometry. Geochim. Cosmochim. Acta 67, 3473–3497.

Hekinian, R., Bideau, D., Cannat, M., Francheteau, J., Hebert, R., 1992. Volcanic activity and crust–mantle exposure in the ultrafast Garrett Transform fault near 13°28′S in the Pacific. Earth Planet. Sci. Lett. 108, 259–275.

Hekinian, R., Bideau, D., Hebert, R., Niu, Y., 1995. Magmatism in the Garrett transform fault (East Pacific Rise near 13°27′S). J. Geophys. Res. 100, 10163–10185.

Hekinian, R., Francheteau, J., Armijo, R., Cogne, J.P., Constantin, M., Giradeau, J., Hey, R., Naar, D.F., Searle, R., 1996. Petrology of the Easter microplate region in the South Pacific. J. Volcanol. Geotherm. Res. 72, 259–289.

Hekinian, R., Stoffers, P., Devey, C., Ackermand, D., Hemmond, C., O'Connor, J., Binard, N., Maia, M., 1997. Intraplate versus ridge volcanism on the Pacific–Antarctic Ridge near 37°S–111°W. J. Geophys. Res. 102, 12265–12286.

Hekinian, R., Stoffers, P., Ackermand, D., Revillon, S., Maia, M., Bohn, M., 1999. Ridge-hotspot interaction: the Pacific–Antarctic Ridge and the Foundation Seamounts. Mar. Geol. 160, 199–223.

Hekinian, R., Stoffers, P., Cheminee, J.-L. (Eds.), 2004. Oceanic Hotspots: Intraplate Submarine Magmatism and Tectonism. Springer, Berlin, Federal Republic of Germany (DEU) pp. 480.

Hirata, N., 1991. Report on DELP 1988 cruises in the Okinawa Trough: Part 3. Crustal Structure of the Southern Okinawa Trough. Bulletin of the Earthquake Research Institute, vol. 66. University of Tokyo, pp. 37–70.

Hofmann, A.W., 1988. Chemical differentiation of the Earth: the relationship between mantle, continental crust, and oceanic crust. Earth Planet. Sci. Lett. 90, 297–314.

Hofmann, A.W., Jochum, K.P., Seufert, M., White, W.M., 1986. Nb and Pb in oceanic basalts: new constraints on mantle evolution. Earth Planet. Sci. Lett. 79, 33–45.

Kamenetsky, V.S., Binns, R.A., Gemmell, J.B., Crawford, A.J., Mernagh, T.P., Maas, R., Steele, D., 2001. Parental basaltic melts and fluids in eastern Manus backarc basin; implications for hydrothermal mineralisation. Earth Planet. Sci. Lett. 184, 685–702.

Keller, R.A., Fisk, M.R., 1992. Quaternary marginal basin volcanism in the Bransfield Strait as a modern analogue of the southern Chilean ophiolites. In: Parson, L.M., Murton, B.J., Browning, P. (Eds.), Ophiolites and their Modern Oceanic Analogues. Special Publications, vol. 60. Geological Society, London, pp. 155–169.

Keller, R.A., Fisk, M.R., White, W.M., Birkenmajer, K., 1992. Isotopic and trace element constraints on mixing and melting models of marginal basin volcanism, Bransfield Strait, Antarctica. Earth Planet. Sci. Lett. 111, 287–303.

Keller, R.A., Fisk, M.R., Smellie, J.L., Strelin, J.A., Lawver, L.A., 2002. Geochemistry of back arc basin volcanism in Bransfield Strait, Antarctica: Subducted contributions and along-axis variations. J. Geophys. Res. 107, ECV 4-1–ECV 4-17.

Klepeis, K.A., Lawver, L.A., 1996. Tectonics of the Antarctic–Scotia plate boundary near Elephant and Clarence Islands, West Antarctica. J. Geophys. Res. 101, 20211–20231.

Klinkhammer, G.P., Chin, C.S., Wilson, C., Rudnicki, M.D., Keller, R.A., Fisk, M.R., Lawver, L.A., 1995. Results of a search for hydrothermal activity in the Bransfield Strait, Antarctica. AGU 1995 Fall Meeting EOS Trans. Am. Geophys. Union, vol. 76, p. 710.

Klinkhammer, G.P., Chin, C.S., Keller, R.A., Daehlmann, A., Sahling, H., Sarthou, G., Petersen, S., Smith, F., Wilson, C., 2001. Discovery of new hydrothermal vent sites in Bransfield Strait, Antarctica. Earth Planet. Sci. Lett. 193, 395–407.

Kohut, E., Nielsen, R.L., 2004. Melt inclusion formation mechanisms and compositional effects in high-An feldspar and high-Fo olivine in anhydrous mafic silicate liquids. Contrib. Mineral. Petrol. 147, 684–704.

Lawver, L.A., Keller, R.A., Fisk, M.R., Strelin, J.A., 1995. Bransfield Strait, Antarctic Peninsula: active extension behind a dead arc. In: Taylor, B.E. (Ed.), Backarc Basins: Tectonics and Magmatism. Plenum Press, New York, pp. 315–342.

Lisitsyn, A.P., Bogdanov, Y.A., Zonenshayn, L.P., Kuz'min, M.I., Sagalevich, A.M., 1989. Hydrothermal phenomena in the Mid-Atlantic ridge at Lat. 26° N (TAG hydrothermal field). Int. Geol. Rev. 31, 1183–1198.

Lu, F., Anderson, A.T., Davis, A.M., 1995. Diffusional gradients at the crystal/melt interface and their effect on the composition of melt inclusions. J. Geol. 103, 591–597.

Lüders, V., Pracejus, B., Halbach, P., 2001. Fluid inclusion and sulfur isotope studies in probable modern analogue Kuroko-type ores from the JADE hydrothermal field (Central Okinawa Trough, Japan). Chem. Geol. 173, 45–58.

Mammerickx, J., 1992. The Foundation Seamounts: tectonic setting of a newly discovered seamount chain in the South Pacific. Earth Planet. Sci. Lett. 113, 293–306.

Mann, P., Hempton, M.R., Gradley, D.C., Burke, K., 1983. Development of pull-apart basins. J. Geol. 91, 529–554.

Martinez, F., Taylor, B., 1996. Back-arc spreading, rifting and microplate rotation, between transform faults in the Manus Basin. Mar. Geophys. Res. 18, 203–224.

Mavrogones, J.A., O'Neill, H.St.C., 1999. The relative effects of pressure, temperature and oxygen fugacity on the solubility of sulfide in mafic magmas. Geochim. Cosmochim. Acta 63, 1173–1180.

McDonough, W.F., Sun, S.S., 1995. Composition of the Earth. Chem. Geol. 120, 223–253.

McDonough, W.F., Sun, S.S., Ringwood, A.E., Jagoutz, E., Hofmann, A.W., 1992. Potassium, rubidium and cesium in the Earth, Moon and the evolution of the mantle of the Earth. Geochim. Cosmochim. Acta 56, 1001–1012.

McGregor, B.A., Harrison, C.G.A., Lavelle, J.W., Rona, P.A., 1977. Magnetic anomaly patterns on Mid-Atlantic Ridge crest at 26°N. J. Geophys. Res. 82, 231–238.

Michael, P.J., Chase, R.L., Allan, J.F., 1989. Petrologic and geologic variations along the southern Explorer Ridgel, Northeast Pacific Ocean. J. Geophys. Res. 94 (10), 13,895–13,918.

Michael, P.J., McDonough, W.F., Nielsen, R.L., Cornell, W.C., 2002. Depleted melt inclusions in MORB plagioclase: messages from the mantle or mirages from the magma chamber? Chem. Geol. 183, 43–61.

Miller, D.M., Goldstein, S.L., Langmuir, C.H., 1994. Cerium/lead and lead isotope ratios in arc magmas and the enrichment of lead in the continents. Nature (London) 368, 514–520.

Moss, R., Scott, S.D., 2001. Geochemistry and mineralogy of gold-rich hydrothermal precipitates from the eastern Manus basin, Papua New Guinea. Can. Mineral. 39, 957–978.

Moss, R., Scott, S.D., Binns, R., 1997. Concentrations of gold and other ore metals in volcanics hosting the PACMANUS seafloor sulfide deposit. JAMSTEC J. Deep-Sea Res. 13, 257–267.

Moss, R., Scott, S.D., Binns, R.A., 2001. Gold content of eastern Manus Basin volcanic rocks; implications for enrichment in associated hydrothermal precipitates. Econ. Geol. Bull. Soc. Econ. Geol. 96, 91–107.

Mungall, J.E., 2002. Roasting the mantle; slab melting and the genesis of major Au and Au-rich Cu deposits. Geology (Boulder) 30, 915–918.

Natland, J.H., 1989. Partial melting of a lithologically heterogeneous mantle: inferences from crystallisation histories of magnesian abyssal tholeiites from the Siqueiros Fracture Zone. In: Saunders, A.D., Norry, M.J. (Eds.), Magmatism in the Ocean Basins Geological Society of London Special Publication, vol. 42, pp. 41–70.

Niedermann, S., Bach, W., Erzinger, J., 1997. Noble gas evidence for a lower mantle component in MORBs from the southern East Pacific Rise: decoupling of helium and neon isotope systematics. Geochim. Cosmochim. Acta 61, 2697–2715.

Nielsen, R.L., Crum, J., Bourgeois, R., Hascall, K., Forsythe, L.M., Fisk, M.R., Christie, D.M., 1995. Melt inclusions in high-An plagioclase from the Gorda Ridge: an example of local diversity of MORB parent magmas. Contrib. Mineral. Petrol. 122, 34–50.

Niu, Y., Batiza, R., 1997. Trace element evidence from the seamounts for recycled oceanic crust in the Eastern Pacific mantle. Earth Planet. Sci. Lett. 148, 471–483.

Niu, Y., Hekinian, R., 1997. Basaltic liquids and harzburgitic residues in the Garrett Transform: a case study at fast-spreading ridges. Earth Planet. Sci. Lett. 146, 243–259.

Pearce, N.J.G., Perkins, W.T., Westgate, J.A., Gorton, M.P., Jackson, S.E., Neal, C.R., Chernery, S.P., 1997. A compilation of new and published major and trace element data for NIST SRM 610 and NIST SRM 612 glass reference materials. Geostand. Newsl., J. Geostand. Geoanal. 21 (1), 115–144.

Pelayo, A.M., Wiens, D.A., 1989. Seismotectonics and relative plate motions in the Scotia Sea region. J. Geophys. Res. 94, 7293–7320.

Perfit, M.R., Fornari, D.J., Ridley, W.I., Kirk, P.D., Casey, J., Kastens, K.A., Reynolds, J.R., Edwards, M., Desonie, D.L., Shuster, R., Paradis, S., 1996. Recent volcanism in the Siqueiros transform fault: picritic basalts and implications for MORB magma genesis. Earth Planet. Sci. Lett. 141, 91–108.

Petersen, S., Herzig, P.M., Hannington, M., 2000. Third dimension of a presently forming VMS deposit: TAG hydrothermal mound, Mid-Atlantic Ridge, 26°N. Miner. Depos. 35, 233–259.

Petersen, S., Herzig, P., Schwarz-Schampera, U., Hannington, M.D., Jonasson, I.R., 2004. Hydrothermal precipitates associated with bimodal volcanism in the Central Bransfield Strait, Antarctica. Miner. Depos. 39, 358–379.

Pettke, T., Halter, W.E., Webster, J.D., Aigner-Torres, M., Heinrich, C.A., 2004. Accurate quantification of melt inclusion chemistry by LA-ICPMS: a comparison with EMP and SIMS and advantages and possible limitations of these methods. Lithos 78, 333–361.

Purdy, G.M., Sempéré, J.C., Schouten, H., Dubois, D.L., Goldsmith, R., 1990. Bathymetry of the Mid-Atlantic Ridge, 24°–31°N: a map series. Mar. Geophys. Res. 12, 247–252.

Rhodes, J.M., Morgan, C., Liias, R.A., 1990. Geochemistry of Axial Seamount lavas; magmatic relationship between the Cobb hotspot and the Juan de Fuca Ridge. In: Johnson, H.P., Embley, W.R. (Eds.), Special Section: Axial Seamount: an Active Ridge Axis Volcano on the Central Juan de Fuca Ridge J. Geophys. Res., vol. 95, pp. 12,713–12,733.

Rona, P.A., Klinkhammer, G.P., Nelsen, T.A., Trefry, J.H., Elderfield, H., 1986. Black smokers, massive sulfides, and vent biota at the Mid-Atlantic Ridge. Nature (London) 321, 33–37.

Rona, P.A., Bogdanov, Y.A., Gurvich, E.G., Rimski-Korsakov, N.A., Sagalevitch, A.M., Hannington, M.D., Thompson, G., 1993a. Relict hydrothermal zones in the TAG hydrothermal field, Mid-Atlantic Ridge, 26°N, 45°W. J. Geophys. Res. 98, 9715–9730.

Rona, P.A., Hannington, M.D., Raman, C.V., Thompson, G., Tivey, M.K., Humphris, S.E., Lalou, C., Petersen, S., 1993b. Active and relict seafloor hydrothermal mineralization at the TAG hydrothermal field, Mid-Atlantic Ridge. Econ. Geol. Bull. Soc. Econ. Geol. 88, 1989–2017.

Rona, P.A., Petersen, S., Becker, K., Von Herzen, R.P., Hannington, M.D., Herzig, P., Lalou, C., Thompson, G., 1996. Heat flow and mineralogy of TAG relict high temperature hydrothermal zones: Mid-Atlantic Ridge 26°N, 45°W. Geophys. Res. Lett. 23, 3507–3510.

Scott, S.D., 1997. Submarine hydrothermal systems and deposits, In: Barnes, H.L. (Ed.), Geochemistry of Hydrothermal Ore Deposits, 3rd edition. John Wiley & Sons, pp. 797–875.

Scott, S.D., Binns, R.A., 1995. Hydrothermal processes and contrasting styles of mineralization in the western Woodlark and eastern Manus basins of the western Pacific. In: Parson, L.M., Walker, C.L., Dixon, D.R. (Eds.), Hydrothermal Vents and Processes. Geological Society Special Publication, London, pp. 191–205.

Scott, S.D., Barrett, T.J., Hannington, M., Chase, R.L., Fouquet, Y., Juniper, S.K., 1984. Tectonic framework and sulfide deposits of southern Explorer Ridge, northeastern Pacific Ocean. AGU 1984 Fall Meeting EOS Trans. Am. Geophys. Union, vol. 65, p. 1111.

Scott, S.D., Hannington, M.D., Chase, R.L., Michael, P.J., 1985. The Explorer Ridge polymetallic sulphide (pms) deposits: a major find in Canadian Pacific waters. Symposium on Marine Mineral Resources. Geological Society of London, p. 11. Abstracts.

Scott, S.D., Chase, R.L., Hannington, M.D., McConachy, T.F., Shea, G.T., 1990. Sulphide deposits, tectonics and petrogenesis of southern Explorer Ridge, Northeast Pacific Ocean. In: Malpas, J., Moores, E.M., Panayiotou, A., Xenophontos, C. (Eds.), Ophiolites; Oceanic Crustal Analogues; Proceedings of the Symposium "Troodos 1987". Ministry of Agriculture and Natural Resources, Nicosia, Cyprus, pp. 719–733.

Sempéré, J.C., Purdy, G.M., Schouten, H., 1990. Segmentation of the Mid-Atlantic Ridge between 24°N and 30°40′N. Nature (London) 344, 427–431.

Shimizu, N., Sobolev, A.V., Layne, G.D., 2000. Large Pb variations in single-lava melt inclusion suites in MORB. Grenoble Melt Inclusion Conference Abstracts.

Shinjo, R., Kato, Y., 2000. Geochemical constraints on the origin of bimodal magmatism at the Okinawa Trough, an incipient back-arc basin. Lithos 54, 117–137.

Shipboard Scientific Party, 2002. Anatomy of an active, felsic-hosted hydrothermal system, eastern Manus basin: Sites 1188–1191, 7 November 2000–3 January 2002. Proceedings of the Ocean Drilling Program. Initial Reports, vol. 193. National Science Foundation and Joint Oceanographic Institutions, Inc. 84 pp.

Sibuet, J.C., Deffontaines, B., Hsu, S.-K., Thareau, N., Le Formal, J.-P., Liu, C.-S., ACT party, 1998. Okinawa trough backarc basin: early tectonic magmatic evolution. J. Geophys. Res. 103, 30245–30267.

Sinton, C.W., Christie, D.M., Coombs, V.L., Nielsen, R.L., Fisk, M.R., 1993. Near primary melt inclusions in anorthite phenocrysts from the Galapagos Platform. Earth Planet. Sci. Lett. 119, 527–537.

Sobolev, A.V., Shimizu, N., 1993. Ultra-depleted primary melt included in an olivine from the Mid Atlantic ridge. Nature 363, 151–154.

Sobolev, A.V., Shimizu, N., 1994. The origin of typical NMORB: the evidence from a melt inclusion study. Mineral. Mag. J. Mineral. Soc. 58A, 862–863.

Sobolev, A.V., Casey, H.F., Shimizu, N., Perfit, M.R., 1992. Contamination and mixing of MORB primary melts: evidence from melt inclusions in Siqueiros picrites. EOS Trans. Am. Geophys. Union 72, 336.

Sobolev, A.V., Gurenko, A., Shimizu, N., 1994. Ultra-depleted melt from Iceland: data from melt inclusion studies. Mineral. Mag. 58A, 860–861.

Sours-Page, R., Nielsen, R.L., Johnson, K.T.M., Karsten, J.L., 1999. Local and regional variation of MORB parent magmas: evidence from melt inclusions from the Endeavour Segment of the Juan de Fuca Ridge. Contrib. Mineral. Petrol. 134, 342–363.

Stolper, E., Newman, S.W., 1994. The role of water in the petrogenesis of Mariana Trough magmas. Earth Planet. Sci. Lett. 121, 293–325.

Sun, S.-S., Nesbitt, R.W., Sharaskin, A.Y., 1979. Geochemical characteristics of mid-ocean ridge basalts. Earth Planet. Sci. Lett. 44, 119–138.

Taylor, B., 1979. Bismarck Sea: evolution of a back-arc basin. Geology 7, 171–174.

Thomas, J.B., Bodnar, R.J., Shimizu, N., Chesner, C., 2002. What boundary layer? Evidence from melt inclusions in plagioclase, quartz, allanite and zircon from the Toba Tuffs, Sumatra, Indonesia. In: Kontak, D.J., Anderson, A.J. (Eds.), Eighth Biennial Pan-American Conference on Research on Fluid Inclusions. Nova Scotia, Halifax, pp. 103–104.

Thompson, G., Humphris, S.E., Schroeder, B., Sulanowska, M., Rona, P.A., 1988. Active vents and massive sulfides at 26°N (TAG) and 23°N (Snake Pit) on the Mid-Atlantic Ridge. Can. Mineral. 26, 697–711.

Verati, C., Lancelot, J., Hekinian, R., 1999. Pb isotope study of black-smokers and basalts from Pito Seamount site (Easter Microplate). In: Moeller, P., Fouquet, Y., Shepherd, T.J. (Eds.), Hydrothermal Systems, Alteration and Ore Deposition Chem. Geol., vol. 155, pp. 45–63.

Walter, H.F., Sandwell, D.T., 1997. Global sea floor topography from satellite altimetry and ship depth soundings. Science 277, 1956–1962.

Wendt, J.I., Regelous, K.D., Hekinian, R., Niu, Y., Collerson, K.D., 1997. The nature of mantle heterogeneities and melt extraction processes beneath the East Pacific Rise (EPR); evidence from ultra-depleted lavas in the Garrett Transform. EOS Trans. Am. Geophys. Union 78, F675.

Wendt, J.I., Regelous, M., Niu, Y., Hekinian, R., Collerson, K.D., 1999. Geochemistry of lavas from the Garrett Transform Fault: insights into mante heterogeneity beneath the eastern Pacific. Earth Planet. Sci. Lett. 173, 271–284.

Yang, K., Scott, S.D., 1996. Possible contribution of a metal-rich magmatic fluid to a sea-floor hydrothermal system. Nature (London) 383, 420–423.

Yang, K., Scott, S.D., 2002. Magmatic degassing of volatiles and ore metals into a hydrothermal system on the modern sea floor of the eastern Manus back-arc basin, western Pacific. Econ. Geol. Bull. Soc. Econ. Geol. 97, 1079–1100.

Yang, K., Scott, S.D., 2005. Vigorous exsolution of volatiles in the magma chamber beneath a hydrothermal system on the modern sea floor of the eastern Manus back-arc basin, western Pacific: Evidence from melt inclusions. Econ. Geol. Bull. Soc. Econ. Geol. 100, 1085–1096.

Yang, K., Scott, S.D., 2006. Magmatic fluids as a source of metals in arc/back-arc hydrothermal systems: evidence from melt inclusions and vesicles. In: Christie, D.M., Fisher, C.R., Lee, S.-M. (Eds.), Back Arc Spreading Systems: Geological, Biological, Chemical and Physical Interactions: American Geophysical Union Geophysical Monograph, vol. 166, pp. 163–184.

Yeats, C.J., Binns, R.A., Parr, J.M., Gemmell, J.B., Scott, S.D., in review. The SuSu Knolls hydrothermal field, Eastern Manus Basin, Papua New Guinea: An actively forming submarine high sulfidation copper–gold system.

Zajacz, Z., Halter, W., 2007. LA-ICPMS analyses of silicate melt inclusions in co-precipitated minerals: Quantification, data analysis and mineral/melt partitioning. Geochim. Cosmochim. Acta 71, 1021–1040.